Bioconjugate Chemistry

pubs.acs.org/bc

Article

Development of an Engineered Single-Domain Antibody for Targeting MET in Non-Small Cell Lung Cancer

Natalie Y. Luo,[#] Rachel L. Minne,[#] Joseph P. Gallant, Gihan S. Gunaratne, Jayden L. West, Saahil Javeri, Austin J. Robertson, Eric W. Lake, Jonathan W. Engle, Jason C. Mixdorf, Eduardo Aluicio-Sarduy, Kwang P. Nickel, Reinier Hernandez, Randall J. Kimple, Andrew M. Baschnagel,* and Aaron M. LeBeau*

Cite This: *Bioconjugate Chem.* 2024, 35, 389−399

Read Online

ACCESS | Metrics & More | Article Recommendations | Supporting Information

ABSTRACT: The Mesenchymal Epithelial Transition (MET) receptor tyrosine kinase is upregulated or mutated in 5% of non-small-cell lung cancer (NSCLC) patients and overexpressed in multiple other cancers. We sought to develop a novel single-domain camelid antibody with high affinity for MET that could be used to deliver conjugated payloads to MET expressing cancers. From a naïve camelid variable-heavy-heavy (VHH) domain phage display library, we identified a VHH clone termed 1E7 that displayed high affinity for human MET and was cross-reactive with MET across multiple species. When expressed as a bivalent human Fc fusion protein, 1E7-Fc was found to selectively bind to EBC-1 (MET amplified) and UW-Lung 21 (MET exon 14 mutated) cell lines by flow cytometry and immunofluorescence imaging. Next, we investigated the ability of [^{89}Zr]Zr-1E7-Fc to detect MET expression *in vivo* by PET/CT imaging. [^{89}Zr]Zr-1E7-Fc demonstrated rapid localization and high tumor uptake in both xenografts with a %ID/g of 6.4 and 5.8 for EBC-1 and UW-Lung 21 at 24 h, respectively. At the 24 h time point, clearance from secondary and nontarget tissues was also observed. Altogether, our data suggest that 1E7-Fc represents a platform technology that can be employed to potentially both image and treat MET-altered NSCLC.

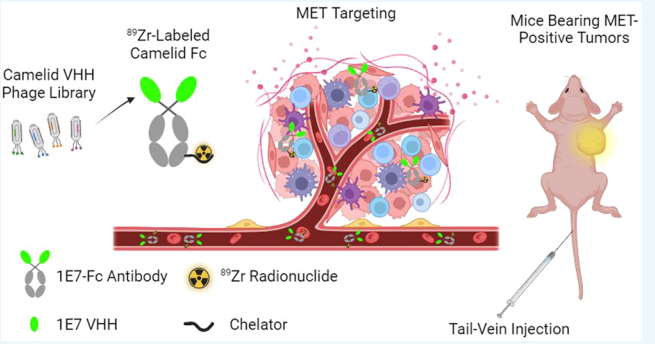

INTRODUCTION

Non-small-cell lung cancer (NSCLC) comprises approximately 85% of all lung cancer cases and is the leading cause of cancer death in the United States. Among the patients with NSCLC, 3−4% have mutated Mesenchymal Epithelial Transition (MET) gene, and 3−6% have an amplified form of this gene.[1,2] MET, also known as c-MET or hepatocyte growth factor receptor (HGFR), is a transmembrane receptor tyrosine kinase that plays a key role in cell proliferation, embryogenesis, tissue development, and wound healing.[3−6] The most common MET mutation occurs in exon 14, which leads to a truncated receptor lacking the Y1003 c-Cbl binding site, resulting in decreased MET protein ubiquitination and increased expression of the MET protein.[7−9] Both MET exon skipping (METex14) mutations and MET amplifications can be targeted with small-molecule inhibitors. Currently, crizotinib, capmatinib, and tepotinib are the three tyrosine kinase inhibitors that are FDA-approved for treating METex14 NSCLC.[10,11] While these therapies are initially effective, resistance inevitably arises, and new, more effective therapies are needed. Since both METex14 mutations and MET amplifications lead to high surface expression and receptor activation, the MET receptor represents an ideal target for antibody-based therapy. A number of monoclonal antibody therapies directed against MET exist in various preclinical and clinical development stages in NSCLC. Thus far, however, results using conventional mono- and polyspecific antibodies against MET have been disappointing with little therapeutic benefit in the clinic.[12−16]

The development of novel therapeutics and the appropriate tailoring of existing therapies for MET amplified and METex14 mutated NSCLC are hindered by the inability to quantify disease burden and patient response to therapy by imaging. The ability to assess MET expression is crucial in selecting patient population for clinical trials investigating MET-targeted therapies. An imaging modality that can accurately and sensitively detect MET-expressing tumors does not exist. Imaging modalities such as CT and MRI are anatomical in nature and inform nothing about the underlying physiology of the tumor.[17] The FDA-approved positron emission tomography (PET) tracer [^{18}F]fluorodeoxyglucose ([^{18}F]FDG) is

Received: January 19, 2024
Revised: February 1, 2024
Accepted: February 1, 2024
Published: March 12, 2024

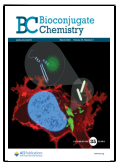

commonly used to imaging a number of different cancer types including NSCLC.[18] The mechanism behind [^{18}F]FDG imaging is based on the Warburg effect whereby cancer cells have higher glycolytic rates and use more glucose than nonmalignant cells.[19] [^{18}F]FDG is not specific for different NSCLC subtypes and cannot delineate between diseases expressing varying levels of MET.[20,21] Additionally, [^{18}F]FDG uptake is nonspecific and can result in false-positive results.[22] No MET-targeted imaging agents are currently undergoing clinical trials. The exposed 45 kDa extracellular domain of MET does, however, lend itself to the development of targeted biologics.

None of the previous studies targeting MET in NSCLC with biologics have explored the use of camelid antibody binding domains. The immune repertoire of the camelidae family (llamas, alpacas, camels, etc.) is unique in that it possesses immunoglobulins that have single-chain only variable regions for antigen engagement rather than canonical heavy-light chain pairs.[23] These camelid binding domains share high homology with human heavy chains and are often referred to as Variable-Heavy-Heavy domains (VHHs).[24] VHHs are characterized by their small size (~15 kDa, 4 nm by 2.5 nm), high solubility, stability, specificity and affinity, and ease of cloning.[25] Their small size allows for greater tissue penetration and rapid clearance from the blood and nontarget tissues.[26] Unlike conventional antibodies that have six total complementary determining regions (CDRs) for antigen engagement, three on each heavy and light chain, VHHs only have three CDRs making them a fraction the size of a conventional heavy-light chain antibody binding domain.[27,28] The CDR3 of VHHs are often 20 amino acids or more and can adopt concave and convex binding conformations leading to high affinity interactions. When grafted onto a human Fc domain, VHH-Fc constructs still only have a molecular weight of 80 kDa, suggesting they may have *in vivo* half-lives that pair well with the positron-emitting radionuclide ^{89}Zr ($t_{1/2}$ − 3.3 d) or the therapeutic radionuclide ^{90}Y ($t_{1/2}$ − 2.7 d). VHHs represent a class of biologics that warrant further investigation as scaffold technologies for nuclear imaging and therapy.

In this study, we document the identification by phage display of a potent VHH domain targeting MET. Our novel VHH-Fc construct, 1E7-Fc, demonstrated high binding affinity to recombinant MET protein and MET-altered NSCLC cell lines through ELISA, biolayer interferometry, flow cytometry, and live cell confocal imaging. *In vivo* experiments confirmed the stability and ability of our VHH-Fc to image MET-altered xenograft models of lung cancer by positron emission tomography (PET). High uptake was observed in the MET-expression xenograft tumors with low uptake in normal tissues, suggesting the potential utility of our VHH-Fc as a diagnostic tool or targeted radiotherapy.

RESULTS

Identification and Characterization of Anti-MET VHH Domains. Single-domain constructs specific to the MET extracellular domain were identified from a naïve VHH antibody phage display library with a diversity of 7.5 × 10^{10}. This library was constructed in-house from B cells isolated from the blood, bone marrow, and spleen tissue of nearly a dozen llamas and alpacas. Library screening was performed against biotinylated human MET immobilized on streptavidin-coated magnetic beads. After four rounds of selection, 384 VHHs were screened against biotinylated human MET by ELISA. A signal threshold of 1.00 was used to identify 12 candidate MET binders by ELISA (Figure 1B). The 12

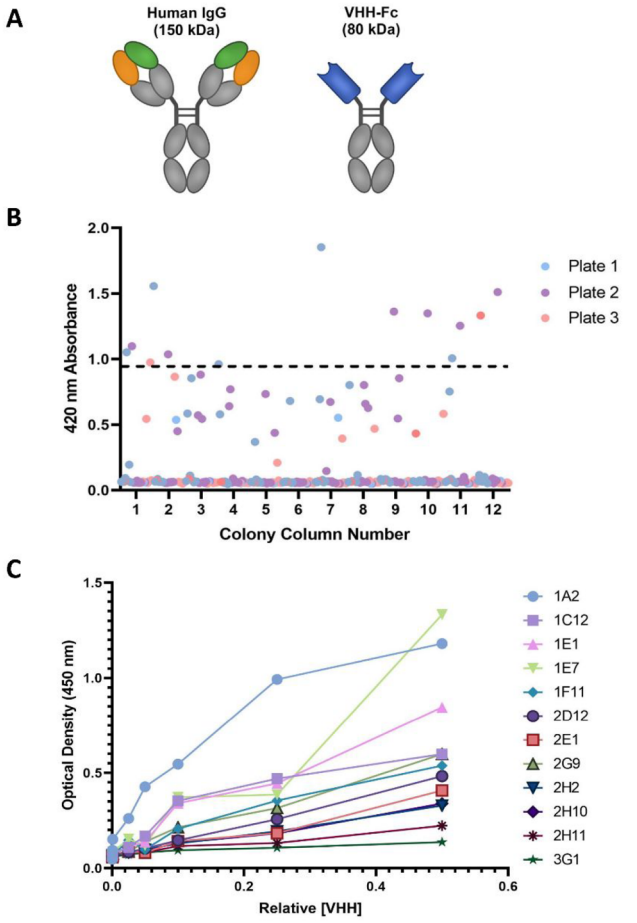

Figure 1. Discovery of potential anti-MET VHHs from a camelid antibody phage display library. (A) Schematic of an IgG antibody and VHH-Fc with their average molecular weights. (B) Screening of VHH clones for MET by ELISA. 384 unpurified VHH clones in culture supernatant were added to wells coated with MET protein. VHH binding was detected using a peroxidase conjugated anti-HA-tag monoclonal antibody and Turbo TMB reagent. Twelve clones with high 420 nm absorbance values (greater than 0.9) were identified. (C) Dilution ELISA of VHH clones demonstrated saturable binding to MET. Twelve unpurified VHHs were serially diluted from 1 to 0.05 relative concentration and added to human MET protein coated plates. Two clones, 1A2 and 1E7, showed saturating ELISA signals.

unpurified VHHs in culture supernatant were serial diluted and evaluated for a saturating ELISA signal (Figure 1C). Three of the 12 clones had unique sequences (Table S1).

Next, we evaluated the ability of our three unique VHH clones to bind murine and rhesus monkey MET by performing ELISA counter screens. The VHHs showed modest cross-reactivity with murine and rhesus macaque MET suggesting they recognized common conserved epitopes (Figure 2A). The three clones were expressed and purified for additional testing to identify a lead VHH. Biolayer interferometry (BLI) was next used to determine the affinity of each VHH domain for MET (Figure 2B). Clone 1E7 demonstrated the highest affinity for MET with a K_D of 27 nM (Figure 2C). When compared to the other clones, 1E7 had the highest k_{on} and the lowest k_{off}, meaning it possessed faster binding and slower dissociation to

https://doi.org/10.1021/acs.bioconjchem.4c00019
Bioconjugate Chem. 2024, 35, 389−399

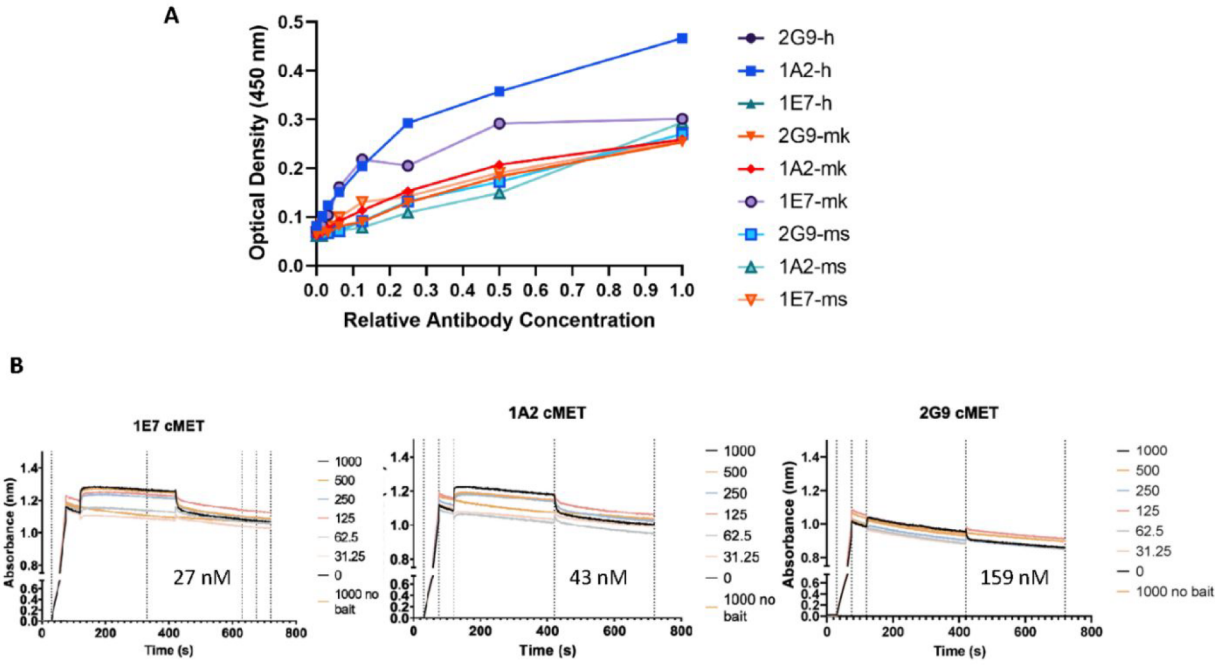

Figure 2. Characterization and selection of 1E7 among three anti-VHHs with high affinity for MET. (A) VHHs' specificity for human (blue), rhesus macaque (orange), and murine (purple) MET was determined by ELISA. Unpurified VHH clones were serially diluted from 1 to 0.00025 and incubated on plates that were coated with the target protein. 1E7 showed saturating ELISA signals on human MET and decreased binding to rhesus macaque and murine MET. (B) Biolayer interferometry (BLI) was used to calculate and compare 1E7, 1A2, and 2G9 binding affinities to human MET. 1E7 demonstrated the highest binding affinity, whereas 1A2 and 2G9 showed weaker binding to human MET.

MET (Table S2). Additionally, 1E7 also had the strongest MET signal in the dilution ELISA for human MET (Figure 1C). The BLI and dilution ELISA data combined determine that 1E7 was the lead clone for development into a VHH-Fc targeting MET.

Generation and in Vitro Characterization of Anti-MET VHH-Fc. 1E7 was cloned into an Fc vector to create a bivalent human Fc construct, 1E7-Fc, with an increased molecular weight of 86.6 kDa. Following expression and purification, the ability of 1E7-Fc to selectively bind to MET-expressing cells was confirmed using multiple *in vitro* approaches. We confirmed that 1E7-Fc only binds to human MET by performing BLI with human MET and other human surface proteins. The lack of binding to other proteins and binding to MET demonstrates 1E7-Fc binds specifically to MET (Figure 3A). Two MET-altered NSCLC cell lines, EBC1 and UW-Lung 21, and two HeLa cell lines, wild type (HeLa WT) and MET knockout (HeLa MET KO), were stained with 1E7-Fc followed by a secondary antibody that was fluorophore labeled for flow cytometry. As indicated by the right shift, 1E7-Fc bound tightly to EBC-1 and UW-Lung 21, moderately to HeLa-WT, and did not bind to HeLa-METKO (Figure 3B). Live cell immunofluorescent imaging was next performed to determine whether 1E7-Fc was internalized in MET-altered NSCLC cell lines after binding to the MET receptor. The cells were incubated with a green CellMask Plasma Membrane Stain followed by treatment with Alexa FluorTM 647-labeled 1E7-Fc. At 2 h post-treatment, 1E7-Fc (red) demonstrated high binding to the cell surface (green) with internalization in UW-Lung 21 and EBC-1, some binding to HeLa WT and no binding to HeLa MET KO. Distinct accumulation within the internal cellular components of MET expressing cell lines is indicative of the internalization of 1E7-Fc (Figure 3C).

To determine if 1E7-Fc by itself was a therapeutic and inhibited MET signaling, as has been seen with other MET antibodies such as onartuzumab and emibetuzumab,[29] we performed a cell proliferation assay and Western blot to query effects of 1E7-Fc on cell behavior and downstream signaling pathways. Cell viability was measured using a panel of the same four cell lines. 1E7-Fc alone had no effect on cell viability even at doses far exceeding binding affinity, suggesting that it was biologically inert (Figure 4A). Consistent with the lack of cell growth inhibition, 1E7-did not impact the phosphorylation of MET (p-MET) and downstream signaling of AKT and ERK (Figure 4B). In contrast, treatment with the FDA-approved MET TKI, capmatinib, blocked MET, AKT, and ERK phosphorylation, as anticipated (Figure 4B). These studies confirmed that 1E7-Fc had no biological effect on MET-expressing cells, and it acted as neither an agonist or antagonist.

***In Vivo* Imaging of MET by PET/CT Imaging.** The biodistribution and ability of 1E7-Fc to localize to MET-expressing lung cancer models was assessed by PET/CT. 1E7-Fc was radiolabeled with zirconium-89 (^{89}Zr) using standard conditions and injected via tail vein into mice bearing EBC-1 and UW-Lung 21 xenografts. The mice were imaged by PET/CT longitudinally at 4, 24, 48, 72, and 96 h postinjection. 2D and 3D PET images were analyzed to illustrate organ distribution of [^{89}Zr]Zr-1E7-Fc (Figure 5A). The PET/CT imaging study documents that, over time, [^{89}Zr]Zr-1E7-Fc accumulates in the tumor and clears from other organs, showing specificity for MET-expressing tissue. *Ex vivo* confirmation of MET expression in EBC-1 and UW-Lung 21 xenografts is demonstrated in the positive immunohistochemistry staining.

https://doi.org/10.1021/acs.bioconjchem.4c00019
Bioconjugate Chem. 2024, 35, 389−399

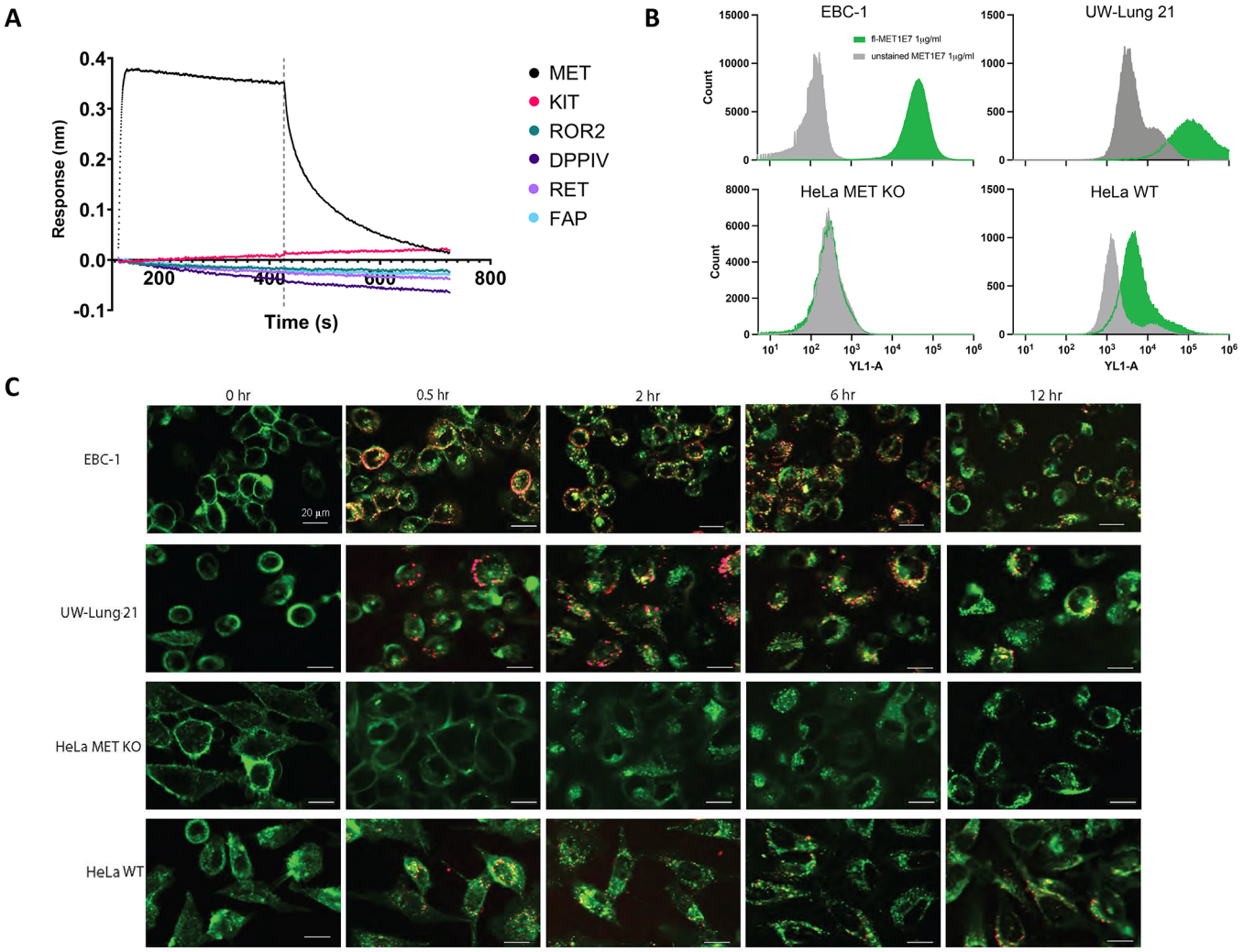

Figure 3. *In vitro* analysis of 1E7-Fc binding specifically to MET-positive cell lines. (A) Confirmation of 1E7-Fc specificity for MET using BLI. 1E7-Fc demonstrated binding only to MET (black line) and minimal to no binding to other surface proteins. (B) 1E7-Fc selectivity for MET-expressing cells was assessed by flow cytometry. Cells were stained with (green) or without (gray) 1E7-Fc at 1 μg/mL. Positive binding is seen in EBC-1, UW-Lung 21, and HeLa WT cells and no MET specificity in HeLa MET KO. (C) Cellular internalization of 1E7-Fc was visualized by immunofluorescent confocal microscopy. Live cells were stained with fluorescent cell plasma membrane dye (green) and treated with 1 mM of 1E7-Fc (red). Accumulation of 1E7-Fc binding is demonstrated in EBC-1 and UW-Lung 21 and moderately in HeLa WT. Scale bar, 20 um.

Analysis of the 3D imaging data confirmed high uptake in the MET-positive xenografts at all time points past 4 h. The data were reconstructed using Inveon Research Workplace to draw Regions of Interest (ROI) around selected organs and obtain the mean percentage injected dose per gram (%ID/g) of tissue. The inverse trend between the heart (blood) and tumor over time demonstrated that the administered [^{89}Zr]Zr-1E7-Fc first traveled to the heart and then localized at the tumor (Figure 6A). The relatively high level of [^{89}Zr]Zr-1E7-Fc in the tumor even at 96 h showed that the antibody is retained in the MET-expressing xenografts (Figure 6A). As illustrated in Figure 5, the radioactive signal in the tumors of both xenografts nearly reached their zenith at 24 h post-injection. In a separate experiment, xenograft-bearing mice were injected with [^{89}Zr]Zr-1E7-Fc, and the organs were harvested 24 h postinjection to determine the biodistribution of the radiolabeled antibody. The tumors of UW-Lung 21 and EBC-1 have high antibody uptake compared to the muscle, digestive system tissues, brain, and bone. The liver, kidney, and spleen also have relatively high uptake as expected because those organs are responsible for filtering the blood (Figure 6B). The high tumor−bone, tumor−muscle, and tumor−brain ratios from the biodistribution data further confirm the localization of [^{89}Zr]Zr-1E7-Fc in MET-positive tumors (Figure 6C).

An *in vivo* stability assay was performed to characterize the viability of 1E7-Fc to stay in the body for therapy and imaging applications. Nontumor bearing mice were injected with 1E7-Fc via the tail vein, and the blood was collected at different time points across a month. Serum was obtained from the collected blood and assessed for levels of residual 1E7-Fc that binds to human MET on a dilution ELISA. Appreciable binding occurred up to 1 week (Figure 6D). This suggests that the 1E7-Fc not only can localize in MET-positive tumors but also is stable enough to be potentially utilized for therapy and imaging.

DISCUSSION

There is a critical unmet need for effective therapies and imaging agents that target MET on the surface of transformed

https://doi.org/10.1021/acs.bioconjchem.4c00019
Bioconjugate Chem. 2024, 35, 389−399

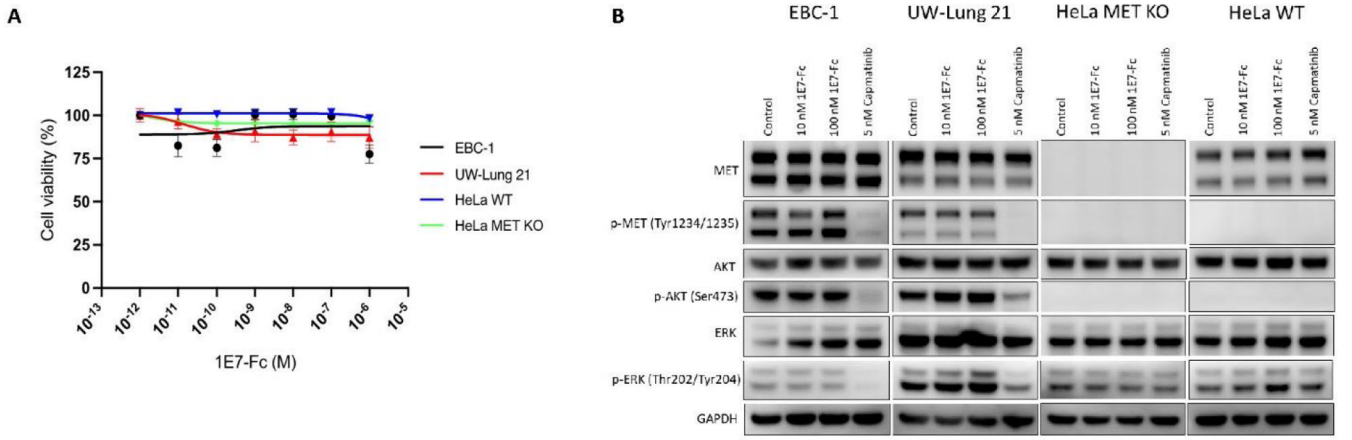

Figure 4. 1E7-Fc does not inhibit cell growth or block MET signaling pathways. (A) Proliferation assay shows that 1E7-Fc does not impact cell survival. The effect of 1E7-Fc on cell viability *in vitro* was assessed for indicated cell lines. Viability was assessed using a Cell Counting Kit-8 cell proliferation assay 72 h after treatment with indicated concentrations of VHH-Fc. Points mean; bar SEM (n = 6). (B) Western blots were performed to assess MET, p-MET (Tyr1234/1235), AKT, p-AKT (Ser473), ERK, p-ERK (Thr202/Tyr204), and GAPDH in cells treated with 1E7-Fc. Cells were treated respective concentrations of 1E7-Fc for 4 h, and Capmatinib (5 nM) was used as a positive control.

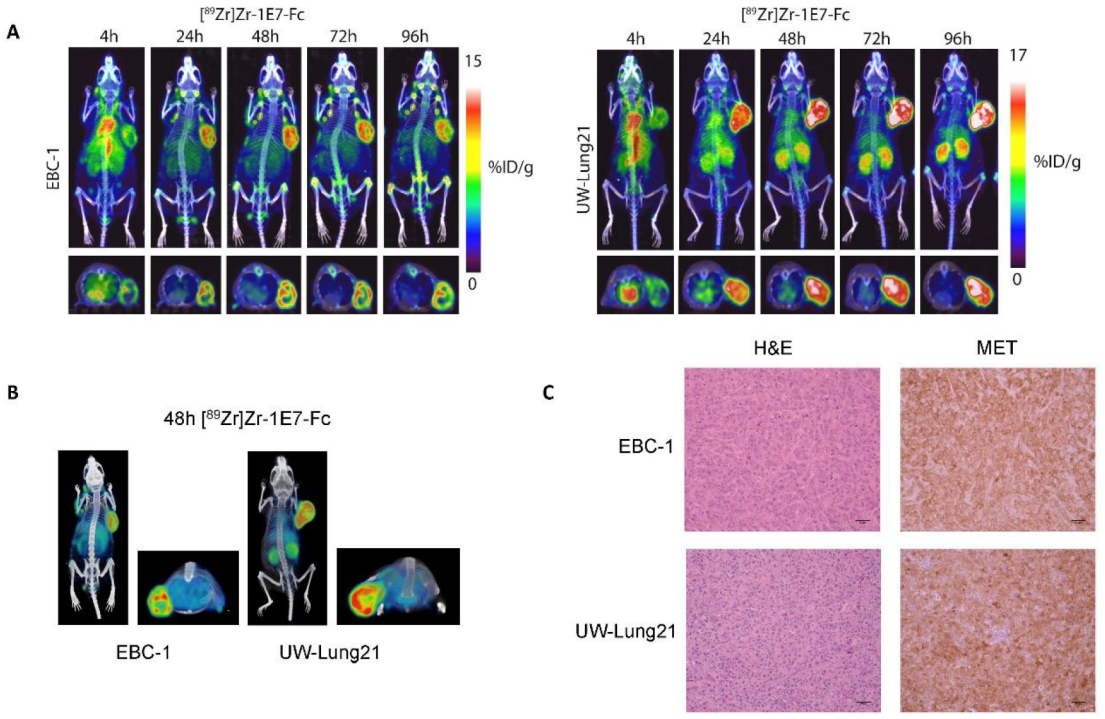

Figure 5. 1E7-Fc targets and accumulates in MET-expressing xenografts. (A) [^{89}Zr]Zr-1E7-Fc can detect MET-positive lung cancer xenografts by PET/CT imaging. Representative PET/CT images of mice bearing EBC-1 and UW-Lung 21 subcutaneous xenografts. Mice (n = 3 per cell line) received around 5.5 MBq [^{89}Zr]Zr-1E7-Fc via tail vein and imaged at the labeled time points. (B) Representative 3D PET/CT images of [^{89}Zr]Zr-1E7-Fc in mice bearing EBC-1 and UW-Lung 21 subcutaneous xenografts at 48 h. (C) *In vivo* validation of MET expression on tumor xenografts. Representative images of MET IHC staining in EBC-1 and UW-Lung 21 xenografts. Scale bar 50 μm.

cells. Therefore, we developed a novel camelid antibody that targets MET, a proto-oncogene, receptor tyrosine kinase, that is upregulated in numerous cancers, including NSCLC. Using a naïve camelid VHH antibody phage display library, we identified our lead clone, 1E7, and subsequently engineered it into a bivalent human Fc fusion protein. 1E7-Fc demonstrated high specificity to MET-positive cell lines based on flow cytometry and confocal microscopy analysis. These results were validated with the *in vivo* xenografts, demonstrating localization and retention of 1E7-Fc in the tumor out to 96 h.

While 1E7-Fc demonstrated high affinity for the MET receptor, it did not have any inhibitory or cytotoxic effect on our MET-expressing cell lines. 1E7-Fc was, however, internalized by MET-expressing cell lines *in vitro*. Internalization is a desired property for PET imaging tracers, radiotherapies, and antibody−drug conjugates to be successful and effective.[30] A PET imaging tracer specific for MET-altered lung cancer does not exist. The most common PET tracer,

https://doi.org/10.1021/acs.bioconjchem.4c00019
Bioconjugate Chem. 2024, 35, 389−399

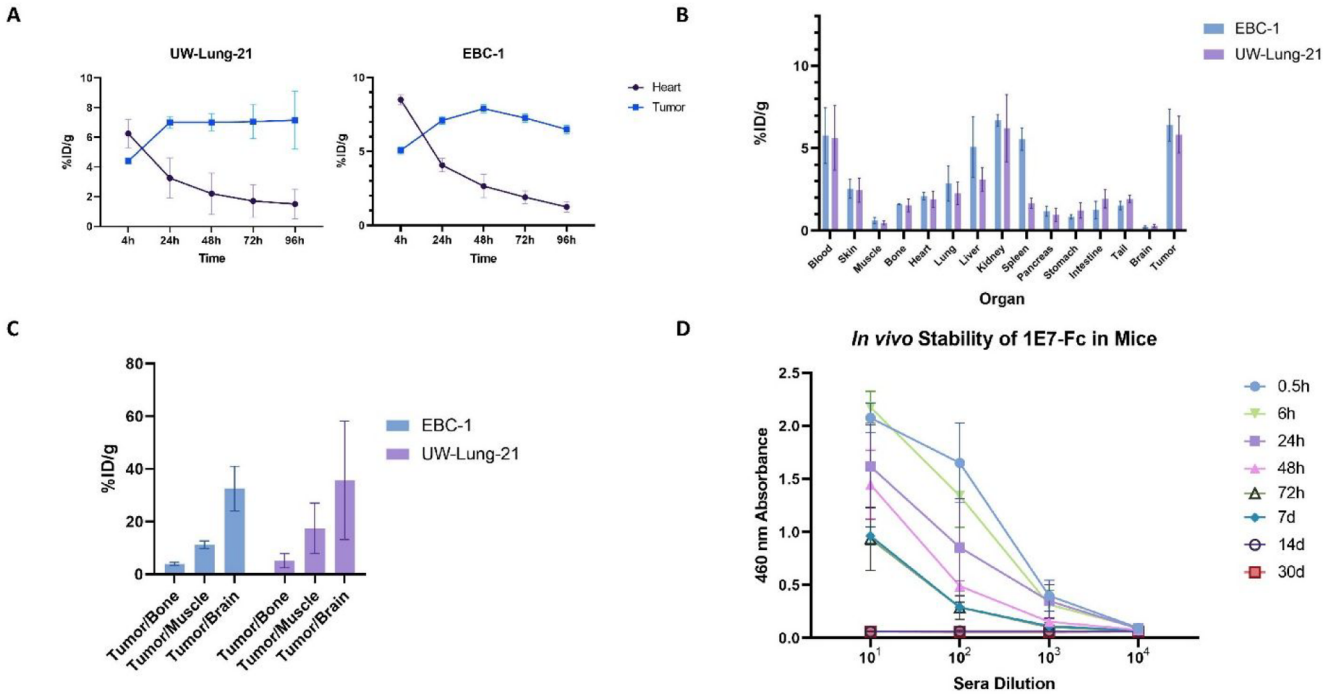

Figure 6. Confirmation of [^{89}Zr]Zr-1E7-Fc selectivity and stability in vivo. (A) Quantitative analysis of the same subcutaneous xenografts as Figure 5. Regions of interest (ROIs) were drawn to obtain values for the heart and tumor for the indicated time points. The inverse relationship between the organs suggests all radiolabeled 1E7-Fc localized in the MET-positive xenograft over time. (B) Biodistribution of [^{89}Zr]Zr1E7-Fc in organs at 24 h. Organs and tissues are harvested at 24 h, and the radioactive counts were measured for each one. There is a significantly higher uptake of [^{89}Zr]Zr-1E7-Fc in the tumor relative to muscle. Values are the mean (n = 3) ± SEM (C) Biodistribution of [^{89}Zr]Zr-1E7-Fc at 24 h in the tumor is significantly higher than in the bone and muscle. Values are the mean (n = 3) ± SEM. (D) In vivo stability of 1E7-Fc is around 3 days. 1E7-Fc was injected into mice via the tail vein, and blood was collected at 8 time points for sera collection. The amount of 1E7-Fc remaining in the sera that binds to human MET was measured with a dilution ELISA. Data are the mean (n = 3) ± SEM.

[^{18}F]FDG, is used to image lung cancer but is limited in its capabilities to specifically detect METexon14 altered NSCLC as the upregulation of glucose consumption is driven by multiple pathways and proteins that are not fully understood.[31] [^{18}F]FDG uptake is also not cancer-specific and results in high background radioactivity in brain tissue.[32] A small-molecule inhibitor of the protease fibroblast activation protein (FAP) labeled with ^{68}Ga has shown greater rates of accurately detecting lung cancer lesions than [^{18}F]FDG, suggesting that there is a possibility for more accurate imaging tracers to better guide treatment decisions.[33] For MET-specific PET tracers, there have been studies with [^{68}Ga]Ga-EMP-100 to target MET in renal cell carcinoma, [^{18}F]F-AH113804 to detect breast cancer, and ^{18}F labeled MET inhibitor for NSCLC.[34−36] These tracers are at different preclinical and clinical stages. None of these are antibody-based tracers nor are they specific for METexon14 NSCLC. Thus, 1E7-Fc represents a platform technology that can exploit the presence of MET on the cell surface to enter the cancer cell to deliver radionuclides for imaging or multiple therapeutic modalities.

A number of antibodies targeting MET that have been developed and investigated for various applications in the clinic. The humanized, one-armed monovalent antihuman MET antibody, onartuzumab, was designed as an antagonist of the MET pathway and performed better than a placebo in a phase II study when combined with erlotinib.[12] However, in phase III clinical trials, there was no improved therapeutic effect when combined with erlotinib compared to erlotinib alone.[37,38] A PET/CT study with onartuzumab showed promising preclinical results of imaging MET when radiolabeled with ^{89}Zr.[39] Emibetuzumab, a humanized antibody, was also investigated in combination with erlotinib in patients with stage IV EGFR mutant NSCLC and in patients with MET positive metastatic NSCLC who acquired resistance to erlotinib. These phase II studies showed no reversal of the erlotinib resistance nor significant clinical benefit.[13,14] Telisotuzumab vedotin (Teliso-V), an antibody−drug conjugate with a microtubule inhibitor warhead, demonstrated antitumor effects during phase I trials. During the phase II trial, Teliso-V had unanticipated toxicity and did not meet the end point of the study.[15,16] Additional constructs, including a murine antibody and human single-chain variable fragments (scFvs) engineered into bivalent cys-diabodies, have been used for imaging MET in preclinical models.[40−42] Curiously, radiotherapy studies using MET-targeted antibodies have never been reported in the literature. Overall, the lack of effective antibodies for targeting MET further underscores the need for new biologic scaffolds and constructs.

To our knowledge, this is the first example in the literature of a VHH being used to image the MET receptor by PET in any cancer type. The data presented demonstrate that 1E7 is a highly selective VHH for human MET. Since 1E7-Fc has no cellular toxicity or effect on other parts of the signaling pathway and is stable *in vivo*, it can be translated as an imaging agent for MET-driven lung cancers without worry of a biological effect. The internalization of 1E7-Fc makes it a promising candidate for use in radioimmunotherapy or as an antibody−drug conjugate. As a VHH, 1E7-Fc has greater stability, a smaller size, and possibly stronger binding to MET than the murine derived scFvs that are undergoing clinical

https://doi.org/10.1021/acs.bioconjchem.4c00019
Bioconjugate Chem. 2024, 35, 389−399

trials. There are many potential future directions for 1E7-Fc to image and treat MET-altered lung cancer, and continuing onto clinical trials is promising.

EXPERIMENTAL PROCEDURES

Cell Culture. Two human NSCLC cell lines expressing MET, HeLa wild type, and the HeLa Met knockout cell line were used in this study. EBC-1 was derived from squamous cell carcinoma, has high MET amplification,[43] and was obtained from JCRB Cell Bank (Xenotech, Kansas City, KS). HeLa wild type and HeLa MET KO cell lines were obtained from Abcam (Waltham, MA, Cat # ab255928 and ab265961, respectively). The UW-Lung 21 PDX was derived from a human lung adenocarcinoma brain metastasis harboring a MET exon 14 skipping mutation. The stable UW-Lung 21 cell line was generated as previously described.[44] Briefly, tumors taken from early UW-Lung 21 patient-derived xenograft (PDX) passages were dissociated into single cell suspensions and seeded in six-well plates containing media (RPMI with 10% fetal bovine serum, 1% L-glutamine, 1% penicillin/streptomycin, and 2.5 μg/mL amphotericin B) and incubated at 37 °C in a humidified atmosphere of 5% CO_2. Media were changed regularly, and cells were passaged once they reached 70% confluence. Mycoplasma testing and short tandem repeat profiling were performed routinely. All cell lines had their identity confirmed via short tandem repeat profiling analysis (Table S3), were maintained, used mycoplasma free at a lower passage, and were cultured as described in Table S4. Capmatinib was purchased from Selleck Chemicals (Houston, TX).

Phage Display Biopanning. A camelid VHH phage display library previously constructed by our lab with a size of 7.5×10^{10} was used to identify single-domain fragments against human MET (ACROBiosystems).[45] Four rounds of bead panning with different amounts of MET antigen (100 μg, 50 μg, and 12.5 μg for the last two rounds) were performed to enrich for binders with high affinity for MET. Phage bound to MET-covered streptavidin beads (Invitrogen) were eluted with 1 mL of 100 mM triethylamine and neutralized with 500 μL 1 M Tris-HCl, pH 7.5. At every round, TG1s were infected with a neutralized phage to proceed to the next round, and at rounds three and four, SS320s were also infected for screening and identifying strong binders.

ELISA. *VHH Screening.* A total of 384 individual clones were selected and produced using 5 mM IPTG induction in a 96-well flat bottom plate. The VHHs released into the supernatant were screened for binding to human cMET by ELISA. MaxiSorp plates (Nunc) were coated with 50 μL of streptavidin (1 μg/mL in PBS, Promega) overnight at 4 °C. The wells were washed twice with PBS and blocked with 2% BSA for 1 h, shaking at room temperature. All proceeding washes were done in PBS and 0.005% Tween20. The wells were washed three times and covered with 50 μL of human cMET (1 μg/mL in PBS) for 1 h, shaking at room temperature. Three washes were done, and the supernatant with released VHH was added to the well (with 1% BSA, 0.005% Tween 20). The plates were shaken for 1 h at room temperature. The wells were washed a final three times, and a 1:1000 dilution of HRP Anti-HA-Proxidase tag antibody (Roche) in PBS, 1% BSA, and 50 μL of Turbo TMB reagent (Pierce) were used. 2.5 M H_2SO_4 was used to stop the reaction. Absorbance at 450 nm was measured with a microplate reader (Tecan), and clones with high absorbance signals were identified as positive cMET binders and sent for sequencing to identify unique sequences.

Dilution ELISA. MaxiSorp plates were prepared as described above. 50 μL of biotinylated human cMET, murine cMET, or rhesus macaque cMET was added to the wells. 1E7 monomeric VHH was serial diluted from 1 μM to 15.6 nM in PBS, 1% BSA, and 0.005% Tween20 and added to each well. Wells with protein but no 1E7 VHH were used as a negative control. 1E7 binding was detected, as described above.

VHH Expression and Purification. Unique nanobodies with high affinity to human c-MET were transformed in Shuffle T7 Competent *Escherichia coli* K12 cells (NEB). Individual colonies were selected and amplified overnight at 37 °C in 100 mL of Terrific Broth (TB) with 100 μg/mL of ampicillin and 0.04% glycerol. The 100 mL overnight cultures were used to inoculate 2 L of TB with 100 μg/mL ampicillin and 0.04% glycerol. Protein expression was induced by adding 1 M IPTC and cultured overnight at 25 °C. Cells were harvested by centrifugation at 5000*g* for 15 min, and the periplasmic *E. coli* fraction was extracted by sonication. The supernatant was obtained after centrifugation at 5000*g* for 30 min and run through a 5 mL HisTrap column (Cytiva). The column was then loaded on a High-Performance Liquid Chromatography machine to purify the VHH into PBS and 10% glycerol. Eluted VHH was combined and concentrated using a 10 kDa centrifugal filter (Millipore) for analysis.

Fc Production and Purification. The 1E7 sequence was cloned into a TGEX human Fc expression vector and transformed into Stellar competent cells (Clontech), and plasmid DNA was purified using PureLink HiPure plasmid maxiprep kits (Thermo Fisher) according to the vendor's recommended protocol. Purified plasmids were then transfected into ExpiCHO-S cells using an Expifectamine CHO Transfection Kit (Thermo Fisher) according to the vendor's recommended protocol, using 1 μg of plasmid DNA and 3.2 μL of Expifectamine CHO Reagent per milliliter of suspension culture. Cells were incubated at 37 °C and 8% CO_2 overnight, shaking at 120 rpm. The next day, transfected cells were supplemented with 6 μL of ExpiCHO Enhancer and 240 μL of ExpiCHO Feed per milliliter of suspension culture, and incubator conditions were changed to 32 °C and 5% CO_2. After 11 days, suspension cultures were harvested and centrifuged at 2000 xrcf for 10 min at 4 °C. The protein-containing supernatant was collected and further clarified by centrifuging at 20 000 xrcf for 30 min at 4 °C and passed through a 0.22 um sterile filter. The 1E7-Fc antibody was captured using protein A and further purified by size exclusion chromatography. A HiTrap Protein A HP column (Cytiva) was equilibrated with five column volumes (CVs) of PBS. Clarified ExpiCHO-S supernatant was supplemented with 300 mM NaCl. Its pH was adjusted to 6.8, and it was pumped onto the protein A column at 1 CV/min. Unbound protein was washed from the column using 10 CVs of PBS. Antibodies were eluted in 2.5 CVs of 100 mM glycine at pH 3.0, followed by 2.5 CVs of PBS. Eluate was immediately neutralized using 2 M Tris HCl at pH 8.6. Eluates were concentrated and buffer exchanged into PBS using an Amicon stirred chamber with a 30 kDa MWCO μL trafiltration membrane (Millipore). Size exclusion chromatography was performed on an ÄKTApure fast protein liquid chromatography system using a HiLoad 16/600 Superdex 200 PG (Cytiva) column equilibrated with PBS. Samples were loaded and fractionated using a mobile phase of PBS at 0.5 mL/min; chromatograms were obtained by

https://doi.org/10.1021/acs.bioconjchem.4c00019
Bioconjugate Chem. 2024, 35, 389−399

monitoring UV absorbance at 280 nm. Eluted protein fractions contributing to a single peak of UV absorbance corresponding to the theoretical molecular mass of 1E7-Fc were collected and pooled. Eluates were diluted to 1 mg/mL in PBS, dispensed into 0.5 mL aliquots, and flash frozen.

Biolayer Interferometry (BLI). Biolayer interferometry was done with the Octet R8 (Sartorius) instrument. Biotinylated human c-MET was captured on a SAX (high precision streptavidin) biosensor. One to four serial dilutions of 1E7-Fc in 1% BSA starting at 1 μM were bound to the biosensor tip with c-MET.

Immunofluorescent Live Cell Imaging. Cells were seeded into an eight-well chamber coverslip slide (#1.5 thickness) at approximately 20 000 to 40 000 cells per well depending on cell type. After incubating at 37 °C for 48 h, cells were stained with a green CellMask Plasma Membrane stain (C37608, Thermo Fisher Scientific) in accordance with the manufacturer procedure. The stained cells were then placed in a temperature- and CO_2-controlled Tokei Hit Biochamber and imaged using a Nikon Ti2 Spinning Disk Confocal Microscope at an objective of 40× with 488 and 547 nm laser settings. At the beginning of the imaging sequence, cells were treated with 1 μM Alexa Fluor 647-labeled 1E7-Fc antibody (A20186, Thermo Fisher Scientific) for 15 m. The cell medium was then suctioned out and phenol red free DMEM media was added (21−063−029, Thermo Fisher Scientific). Images were acquired immediately prior to treatment and 0.5, 2, 6, and 12 h after treatment. Images were processed using Nikon NIS-Elements imaging software and ImageJ.

Flow Cytometry. Cells were harvested with Trypsin for 5 min at 37 °C and 5% CO_2. 1×10^6 cells per condition were incubated with 1 μg/mL of 1E7 Fc for 1 h on ice. Cells were washed and stained with 5 μg/mL goat anti-Human IgG Fc, PE for 1 h on ice. Cells were washed three times and resuspended in flow cytometry staining buffer (eBioscience). Data were collected with the Attune Flow Cytometer (ThermoFisher), and at least 10 000 viable cells were gated and analyzed with FlowJo software.

Cell Proliferation. Cells were plated in 96-well plates at densities ranging from 3000 to 6000 cells per well according to each cell growth rate. Twenty-four hours after-plating, cells were treated with indicated doses of 1E7-Fc or control (PBS) and incubated for 72 h. After 72 h of drug treatment, Cell Counting Kit-8 reagent was added (Dojindo Molecular Technologies) and absorbance measured at 450 nm on a SpectraMax i3 plate reader (Molecular Devices). The absorbance of treated wells was normalized to control wells, and the half-maximal inhibitory concentration (IC50) values were calculated using GraphPad Prism.

Western Blot. Cells were seeded in 10 cm dishes and treated with either control (PBS), 10 nM, or 100 nM 1E7-Fc when cells reached about 75% confluency, and then cells were harvested 4 h after treatment. Five nanomolar Capmatinib was used as a positive control. Cell lysates were generated as previously described.[46] The specific antibodies and sources are listed in Table S5.

Animal Models. All animal studies were conducted under a protocol approved by the University of Wisconsin Institutional Animal Care and Use Committee. Three-to-four-week-old homozygous Foxn1∧nu athymic nude female mice were purchased from Envigo for biodistribution and nuclear imaging studies. Xenografts (n = 3/cell line) were made by injecting each cell line (1×10^6 cells/mL; 100 uL per mouse) in 50% matrigel subcutaneously above the right shoulder blade. Tumors were allowed to grow for 5 weeks for the nuclear imaging experiment.

In Vivo Stability of 1E7. Five-week-old BALB/cJ white mice were purchased from Envigo for in vivo stability study. Mice were intravenously injected through the tail vein with 1E7-Fc (100 μg in 100 μL PBS). Mice were euthanized, and whole blood was collected at 10 different time points. Mouse sera were collected by centrifuging the whole blood at 1500g for 10 min. The sera were then used in ELISA to evaluate their binding to human c-MET.

Bioconjugation and Radiochemistry. 1E7 Fc was conjugated to p-SCN-Bn-deferoxamine (DFO) as described previously.[47] Zirconium-89 [89Zr] was purchased from the University of Wisconsin Medical Physics Department (Madison, WI). [89Zr]Zr-oxalate in 1.0 mol/L oxalic acid was adjusted to pH 7.5 with 1.0 mol/L Na_2CO_3. To radiolabel the 1E7-Fc, the DFO-1E7-Fc conjugate in 0.5 mol/L HEPES (pH 7.5) was added to the neutralized [89Zr]Zr-oxalate solution and incubated at room temperature with rotation for 1 h. A size-exclusion PD-10 column pre-equilibrated with PBS buffer was used to purify the labeled 1E7-Fc. A radiochemical purity of >90% was determined by radioactive TLC using standard methods as described previously.[48] Briefly, the completed reaction was spotted on TLC Silica Gel 60 F_{254} aluminum sheets (EMD Millipore), and 50 mmol/L EDTA (pH 5.0) was used as the eluent. Data were acquired using PerkinElmer Cyclone Plus.

Biodistribution. Nanobodies were labeled with [89Zr] and injected into five-to-six-week-old female Foxn1∧nu athymic nude mice (Envigo) by tail vein injection. Mice (n = 3 mice for each tissue per time point) were euthanized at 4, 24, 48, 72, and 96 h postinjection. Organs and tumors were harvested and evaluated on an automatic gamma-counter (Hidex). The total counts per minute (cpm) of every organ was compared with a standard syringe of known activity and mass. Count data were background- and decay-corrected, and the percentage injected dose per gram (%ID/g) for each tissue sample was calculated by normalization to the total amount of activity injected into each mouse.

PET/CT Imaging. Images were acquired on an Inveon uPET/CT Scanner (Siemens Medical Solutions). Mice (n = 3 for experimental and control groups) were injected with [89Zr]Zr-1E7 Fc by tail vein injection. Mice were anesthetized by inhaling 2.5% isoflurane. Images were recorded at 4, 24, 48, and 96 h time points. PET list mode data were acquired for 80 million counts using a gamma ray energy window of 350−650 keV and coincidence timing window of 3.428 ns. A CT-based attenuation correction was performed for approximately 10 min with 80 kVp, 1 mA, 220 rotation degrees in 120 rotation steps, and 250 ms of exposure time and subsequently reconstructed using a Shepp-Logan filter with 210 μm isotropic voxels. Scans were reconstructed using three-dimensional ordered-subset expectation maximization (two iterations, 16 subsets) with a maximum a posteriori probability algorithm (OSEM3DMAP). Two-dimensional (2D) images and maximum intensity projections (MIPs) were analyzed in Inveon Research Workplace, and ROIs were manually drawn and quantified in Inveon Research Workspace.

Immunohistochemistry. Tumor tissues from EBC-1 and UW-Lung 21 xenografts were fixed in 10% neutral-buffered formalin and embedded in paraffin blocks. Briefly, 5-μm sections were deparaffinized with xylene and hydrated through

https://doi.org/10.1021/acs.bioconjchem.4c00019
Bioconjugate Chem. 2024, 35, 389−399

graded solutions of ethanol. Antigen retrieval was conducted in sodium citrate retrieval buffer (pH 6.0) followed by washing in running water. The slides were washed in PBS and incubated with a 0.3% hydrogen peroxide solution. Blocking was carried out using 10% goat serum in PBS and then was incubated with MET antibody (CST #8198, 1:300) diluted in 1% goat serum in PBS containing 0.1% Triton X-100 overnight at 4 °C. The slides were washed with PBS the next day and then incubated in the secondary antibody (Signal Stain Boost IHC Detection Reagent, CST #8114) for 30 min. Staining was detected using diaminobenzidine (Vector Laboratories #SK-4100). The slides were counterstained with hematoxylin and then dehydrated in ethanol and xylene. Coverslipped sections were imaged on an Olympus BX51 microscope.

■ ASSOCIATED CONTENT

Supporting Information

The Supporting Information is available free of charge at https://pubs.acs.org/doi/10.1021/acs.bioconjchem.4c00019.

Contains Tables S1−S5 (PDF)

■ AUTHOR INFORMATION

Corresponding Authors

Andrew M. Baschnagel − *University of Wisconsin Carbone Cancer Center and Department of Human Oncology, University of Wisconsin School of Medicine and Public Health, Madison, Wisconsin 53792, United States*; Phone: 608-262-9169; Email: baschnagel@humonc.edu

Aaron M. LeBeau − *Department of Pathology and Laboratory Medicine, University of Wisconsin School of Medicine and Public Health, Madison, Wisconsin 53792, United States; University of Wisconsin Carbone Cancer Center and Department of Radiology, University of Wisconsin School of Medicine and Public Health, Madison, Wisconsin 53792, United States*; orcid.org/0000-0003-3802-7789; Phone: 608-262-5586; Email: aaron.lebeau@wisc.edu

Authors

Natalie Y. Luo − *Department of Pathology and Laboratory Medicine, University of Wisconsin School of Medicine and Public Health, Madison, Wisconsin 53792, United States; University of Wisconsin Carbone Cancer Center, University of Wisconsin School of Medicine and Public Health, Madison, Wisconsin 53792, United States*

Rachel L. Minne − *University of Wisconsin Carbone Cancer Center and Department of Human Oncology, University of Wisconsin School of Medicine and Public Health, Madison, Wisconsin 53792, United States*

Joseph P. Gallant − *Department of Pathology and Laboratory Medicine, University of Wisconsin School of Medicine and Public Health, Madison, Wisconsin 53792, United States; University of Wisconsin Carbone Cancer Center and Molecular and Cellular Pharmacology Program, University of Wisconsin School of Medicine and Public Health, Madison, Wisconsin 53792, United States*

Gihan S. Gunaratne − *Department of Pathology and Laboratory Medicine, University of Wisconsin School of Medicine and Public Health, Madison, Wisconsin 53792, United States; University of Wisconsin Carbone Cancer Center, University of Wisconsin School of Medicine and Public Health, Madison, Wisconsin 53792, United States*

Jayden L. West − *Department of Pathology and Laboratory Medicine, University of Wisconsin School of Medicine and Public Health, Madison, Wisconsin 53792, United States; University of Wisconsin Carbone Cancer Center and Molecular and Cellular Pharmacology Program, University of Wisconsin School of Medicine and Public Health, Madison, Wisconsin 53792, United States*

Saahil Javeri − *Department of Human Oncology, University of Wisconsin School of Medicine and Public Health, Madison, Wisconsin 53792, United States*

Austin J. Robertson − *Department of Pathology and Laboratory Medicine, University of Wisconsin School of Medicine and Public Health, Madison, Wisconsin 53792, United States; University of Wisconsin Carbone Cancer Center and Molecular and Cellular Pharmacology Program, University of Wisconsin School of Medicine and Public Health, Madison, Wisconsin 53792, United States*

Eric W. Lake − *Department of Pathology and Laboratory Medicine, University of Wisconsin School of Medicine and Public Health, Madison, Wisconsin 53792, United States; University of Wisconsin Carbone Cancer Center, University of Wisconsin School of Medicine and Public Health, Madison, Wisconsin 53792, United States*

Jonathan W. Engle − *University of Wisconsin Carbone Cancer Center and Department of Human Oncology, University of Wisconsin School of Medicine and Public Health, Madison, Wisconsin 53792, United States*; orcid.org/0000-0002-3399-7228

Jason C. Mixdorf − *University of Wisconsin Carbone Cancer Center, University of Wisconsin School of Medicine and Public Health, Madison, Wisconsin 53792, United States*

Eduardo Aluicio-Sarduy − *University of Wisconsin Carbone Cancer Center, University of Wisconsin School of Medicine and Public Health, Madison, Wisconsin 53792, United States*

Kwang P. Nickel − *University of Wisconsin Carbone Cancer Center and Department of Human Oncology, University of Wisconsin School of Medicine and Public Health, Madison, Wisconsin 53792, United States*

Reinier Hernandez − *University of Wisconsin Carbone Cancer Center and Department of Radiology, University of Wisconsin School of Medicine and Public Health, Madison, Wisconsin 53792, United States*; orcid.org/0000-0002-0729-2179

Randall J. Kimple − *University of Wisconsin Carbone Cancer Center and Department of Human Oncology, University of Wisconsin School of Medicine and Public Health, Madison, Wisconsin 53792, United States*; orcid.org/0000-0001-8336-8000

Complete contact information is available at: https://pubs.acs.org/10.1021/acs.bioconjchem.4c00019

Author Contributions

#N.L. and R.M. contributed equally to this paper.

Notes

The authors declare the following competing financial interest(s): R.H., R.J.K., A.M.B., and A.M.L. are inventors on U.S. provisional patent USPTO-231009-0984.411.

■ ACKNOWLEDGMENTS

This project was supported in part by the University of Wisconsin Carbone Cancer Center Support Grant (P30 CA014520), University of Wisconsin Lung Disease-Oriented Team, donor funds from John Hallick and the MET Crusaders,

NIH/NCI R01 CA237272 (A.M.L.), NIH/NCI R01 CA233562 (A.M.L.), a 2018 Prostate Cancer Foundation Challenge Award (A.M.L.), a Prostate Cancer Foundation Young Investigator Award (A.M.L.), and Andy North and Friends. Figure 1A and Table of Contents graphic were created with BioRender.com.

REFERENCES

(1) Digumarthy, S. R.; Mendoza, D. P.; Zhang, E. W.; Lennerz, J. K.; Heist, R. S. Clinicopathologic and Imaging Features of Non-Small-Cell Lung Cancer with MET Exon 14 Skipping Mutations. *Cancers* **2019**, *11*, 2033.

(2) Okuda, K.; Sasaki, H.; Yukiue, H.; Yano, M.; Fujii, Y. Met gene copy number predicts the prognosis for completely resected non-small cell lung cancer. *Cancer Science* **2008**, *99*, 2280−2285.

(3) Birchmeier, C.; Gherardi, E. Developmental roles of HGF/SF and its receptor, the c-Met tyrosine kinase. *Trends in Cell Biology* **1998**, *8*, 404−410.

(4) Reungwetwattana, T.; Liang, Y.; Zhu, V.; Ou, S.-H. I. The race to target MET exon 14 skipping alterations in non-small cell lung cancer: The Why, the How, the Who, the Unknown, and the Inevitable. *Lung Cancer* **2017**, *103*, 27−37.

(5) Birchmeier, C.; Birchmeier, W.; Gherardi, E.; Vande Woude, G. F. Met, metastasis, motility and more. *Nat. Rev. Mol. Cell Biol.* **2003**, *4*, 915−925.

(6) Trusolino, L.; Bertotti, A.; Comoglio, P. M. MET signalling: principles and functions in development, organ regeneration and cancer. *Nat. Rev. Mol. Cell Biol.* **2010**, *11*, 834−848.

(7) Comprehensive molecular profiling of lung adenocarcinoma. *Nature* **2014**, *511*, 543−550,.

(8) Peschard, P.; Fournier, T. M.; Lamorte, L.; Naujokas, M. A.; Band, H.; Langdon, W. Y.; Park, M. Mutation of the c-Cbl TKB Domain Binding Site on the Met Receptor Tyrosine Kinase Converts It into a Transforming Protein. *Mol. Cell* **2001**, *8*, 995−1004.

(9) Rolle, C. E.; Tan, Y.-H. C.; Seiwert, T. Y.; Vora, S.; Kanteti, R.; Hasina, R.; Carey, G. B.; Surati, M.; Weichselbaum, R. R.; Lingen, M. W.; Vokes, E. E.; Salgia, R. Expression and mutational analysis of c-CBL and its relationship to the MET receptor in head and neck squamous cell carcinoma. *Oncotarget* **2017**, *8*, 18726.

(10) Desai, A.; Cuellar, S. The Current Landscape for METex14 Skipping Mutations in Non-Small Cell Lung Cancer. *J. Adv. Pract Oncol* **2022**, *13*, 539−544.

(11) Hong, L.; Zhang, J.; Heymach, J. V.; Le, X. Current and future treatment options for MET exon 14 skipping alterations in non-small cell lung cancer. *Ther. Adv. Med. Oncol.* **2021**, *13*, No. 175883592199297.

(12) Spigel, D. R.; Edelman, M. J.; O'Byrne, K.; Paz-Ares, L.; Mocci, S.; Phan, S.; Shames, D. S.; Smith, D.; Yu, W.; Paton, V. E.; et al. Results From the Phase III Randomized Trial of Onartuzumab Plus Erlotinib Versus Erlotinib in Previously Treated Stage IIIB or IV Non−Small-Cell Lung Cancer: METLung. *Journal of Clinical Oncology* **2017**, *35*, 412−420.

(13) Camidge, D. R.; Moran, T.; Demedts, I.; Grosch, H.; Mileham, K.; Molina, J.; Juan-Vidal, O.; Bepler, G.; Goldman, J. W.; Park, K.; et al. A Randomized, Open-Label Phase II Study Evaluating Emibetuzumab Plus Erlotinib and Emibetuzumab Monotherapy in MET Immunohistochemistry Positive NSCLC Patients with Acquired Resistance to Erlotinib. *Clinical Lung Cancer* **2022**, *23*, 300−310.

(14) Scagliotti, G.; Moro-Sibilot, D.; Kollmeier, J.; Favaretto, A.; Cho, E. K.; Grosch, H.; Kimmich, M.; Girard, N.; Tsai, C.-M.; Hsia, T.-C.; et al. A Randomized-Controlled Phase 2 Study of the MET Antibody Emibetuzumab in Combination with Erlotinib as First-Line Treatment for EGFR Mutation-Positive NSCLC Patients. *J. Thorac Oncol* **2020**, *15*, 80−90.

(15) Camidge, D. R.; Morgensztern, D.; Heist, R. S.; Barve, M.; Vokes, E.; Goldman, J. W.; Hong, D. S.; Bauer, T. M.; Strickler, J. H.; Angevin, E.; et al. Phase I Study of 2- or 3-Week Dosing of Telisotuzumab Vedotin, an Antibody-Drug Conjugate Targeting c-Met, Monotherapy in Patients with Advanced Non-Small Cell Lung Carcinoma. *Clin. Cancer Res.* **2021**, *27*, 5781−5792.

(16) Waqar, S. N.; Redman, M. W.; Arnold, S. M.; Hirsch, F. R.; Mack, P. C.; Schwartz, L. H.; Gandara, D. R.; Stinchcombe, T. E.; Leighl, N. B.; Ramalingam, S. S.; et al. A Phase II Study of Telisotuzumab Vedotin in Patients With c−MET-positive Stage IV or Recurrent Squamous Cell Lung Cancer (LUNG-MAP Sub-study S1400K, NCT03574753). *Clinical Lung Cancer* **2021**, *22*, 170−177.

(17) Panunzio, A.; Sartori, P. Lung Cancer and Radiological Imaging. *Curr. Radiopharm* **2020**, *13*, 238−242.

(18) Hofman, M. S.; Hicks, R. J. How We Read Oncologic FDG PET/CT. *Cancer Imaging* **2016**, *16*, 35.

(19) Feng, H.; Wang, X.; Chen, J.; Cui, J.; Gao, T.; Gao, Y.; Zeng, W. Nuclear Imaging of Glucose Metabolism: Beyond (18)F-FDG. *Contrast Media Mol. Imaging* **2019**, *2019*, No. 7954854.

(20) Volpi, S.; Ali, J. M.; Tasker, A.; Peryt, A.; Aresu, G.; Coonar, A. S. The role of positron emission tomography in the diagnosis, staging and response assessment of non-small cell lung cancer. *Ann. Transl Med.* **2018**, *6*, 95.

(21) Yousefi-Koma, A.; Panah-Moghaddam, M.; Kalff, V. The Utility of Metabolic Imaging by 18F-FDG PET/CT in Lung Cancer: Impact on Diagnosis and Staging. *Tanaffos* **2013**, *12*, 16−25.

(22) Feng, M.; Yang, X.; Ma, Q.; He, Y. Retrospective analysis for the false positive diagnosis of PET-CT scan in lung cancer patients. *Medicine (Baltimore)* **2017**, *96*, No. e7415.

(23) Riechmann, L.; Muyldermans, S. Single domain antibodies: comparison of camel VH and camelised human VH domains. *J. Immunol Methods* **1999**, *231*, 25−38.

(24) Muyldermans, S. Single domain camel antibodies: current status. *J. Biotechnol.* **2001**, *74*, 277−302.

(25) Van Audenhove, I.; Gettemans, J. Nanobodies as Versatile Tools to Understand, Diagnose, Visualize and Treat Cancer. *EBioMedicine* **2016**, *8*, 40−48.

(26) Arbabi-Ghahroudi, M. Camelid Single-Domain Antibodies: Promises and Challenges as Lifesaving Treatments. *Int. J. Mol. Sci.* **2022**, *23*, 5009.

(27) Muyldermans, S. Applications of Nanobodies. *Annual Review of Animal Biosciences* **2021**, *9*, 401−421.

(28) Konning, D.; Zielonka, S.; Grzeschik, J.; Empting, M.; Valldorf, B.; Krah, S.; Schroter, C.; Sellmann, C.; Hock, B.; Kolmar, H. Camelid and shark single domain antibodies: structural features and therapeutic potential. *Curr. Opin Struct Biol.* **2017**, *45*, 10−16.

(29) De Mello, R. A.; Neves, N. M.; Amaral, G. A.; Lippo, E. G.; Castelo-Branco, P.; Pozza, D. H.; Tajima, C. C.; Antoniou, G. The Role of MET Inhibitor Therapies in the Treatment of Advanced Non-Small Cell Lung Cancer. *Journal of Clinical Medicine* **2020**, *9*, 1918.

(30) Trail, P. A. Antibody Drug Conjugates as Cancer Therapeutics. *Antibodies* **2013**, *2*, 113−129.

(31) Salas, J. R.; Clark, P. M. Signaling Pathways That Drive ^{18} F-FDG Accumulation in Cancer. *J. Nucl. Med.* **2022**, *63*, 659.

(32) Yi, C. A.; Shin, K. M.; Lee, K. S.; Kim, B.-T.; Kim, H.; Kwon, O. J.; Choi, J. Y.; Chung, M. J. Non−Small Cell Lung Cancer Staging: Efficacy Comparison of Integrated PET/CT versus 3.0-T Whole-Body MR Imaging. *Radiology* **2008**, *248*, 632−642.

(33) Wang, L.; Tang, G.; Hu, K.; Liu, X.; Zhou, W.; Li, H.; Huang, S.; Han, Y.; Chen, L.; Zhong, J.; et al. Comparison of 68Ga-FAPI and 18F-FDG PET/CT in the Evaluation of Advanced Lung Cancer. *Radiology* **2022**, *303*, 191−199.

(34) Arulappu, A.; Battle, M.; Eisenblaetter, M.; McRobbie, G.; Khan, I.; Monypenny, J.; Weitsman, G.; Galazi, M.; Hoppmann, S.; Gazinska, P.; Wulaningsih, W.; Dalsgaard, G. T.; Macholl, S.; Ng, T. c-Met PET Imaging Detects Early-Stage Locoregional Recurrence of Basal-Like Breast Cancer. *J. Nucl. Med.* **2016**, *57*, 765.

(35) Mittlmeier, L. M.; Todica, A.; Gildehaus, F. J.; Unterrainer, M.; Beyer, L.; Brendel, M.; Albert, N. L.; Ledderose, S. T.; Vettermann, F. J.; Schott, M.; et al. (68)Ga-EMP-100 PET/CT-a novel ligand for visualizing c-MET expression in metastatic renal cell carcinoma-first in-human biodistribution and imaging results. *Eur. J. Nucl. Med. Mol. Imaging* **2022**, *49*, 1711−1720.

https://doi.org/10.1021/acs.bioconjchem.4c00019
Bioconjugate Chem. 2024, 35, 389−399

(36) Zhaoguo, H.; Tao, Z.; Mingxing, K.; Lina, Q.; Zhexi, W.; Zhengqi, G.; Zibo, L.; Zhanhong, W.; Xilin, S. PET imaging of c-Met activity in NSCLC using ^{18}F Labelled c-MET inhibitor. *J. Nucl. Med.* **2021**, *62*, 148.
(37) Spigel, D. R.; Ervin, T. J.; Ramlau, R. A.; Daniel, D. B.; Goldschmidt, J. H.; Blumenschein, G. R.; Krzakowski, M. J.; Robinet, G.; Godbert, B.; Barlesi, F.; et al. Randomized Phase II Trial of Onartuzumab in Combination With Erlotinib in Patients With Advanced Non−Small-Cell Lung Cancer. *Journal of Clinical Oncology* **2013**, *31*, 4105−4114.
(38) Jagoda, E. M.; Lang, L.; Bhadrasetty, V.; Histed, S.; Williams, M.; Kramer-Marek, G.; Mena, E.; Rosenblum, L.; Marik, J.; Tinianow, J. N.; Merchant, M.; Szajek, L.; Paik, C.; Cecchi, F.; Raffensperger, K.; Jose-Dizon, J.-M.; Bottaro, D. P.; Choyke, P. Immuno-PET of the Hepatocyte Growth Factor Receptor Met Using the 1-Armed Antibody Onartuzumab. *J. Nucl. Med.* **2012**, *53*, 1592.
(39) Pool, M.; Terwisscha van Scheltinga, A. G. T.; Kol, A.; Giesen, D.; de Vries, E. G. E.; Lub-de Hooge, M. N. 89Zr-Onartuzumab PET imaging of c-MET receptor dynamics. *European Journal of Nuclear Medicine and Molecular Imaging* **2017**, *44*, 1328−1336.
(40) Perk, L. R.; Stigter-van Walsum, M.; Visser, G. W. M.; Kloet, R. W.; Vosjan, M. J. W. D.; Leemans, C. R.; Giaccone, G.; Albano, R.; Comoglio, P. M.; van Dongen, G. A. M. S. Quantitative PET imaging of Met-expressing human cancer xenografts with 89Zr-labelled monoclonal antibody DN30. *European Journal of Nuclear Medicine and Molecular Imaging* **2008**, *35*, 1857−1867.
(41) Martinelli, I.; Modica, C.; Chiriaco, C.; Basilico, C.; Hughes, J. M.; Corso, S.; Giordano, S.; Comoglio, P. M.; Vigna, E. hOA-DN30: a highly effective humanized single-arm MET antibody inducing remission of 'MET-addicted' cancers. *J. Exp Clin Cancer Res.* **2022**, *41*, 112.
(42) Li, K.; Tavaré, R.; Zettlitz, K. A.; Mumenthaler, S. M.; Mallick, P.; Zhou, Y.; Marks, J. D.; Wu, A. M. Anti-MET ImmunoPET for Non−Small Cell Lung Cancer Using Novel Fully Human Antibody Fragments. *Molecular Cancer Therapeutics* **2014**, *13*, 2607−2617.
(43) Lutterbach, B.; Zeng, Q.; Davis, L. J.; Hatch, H.; Hang, G.; Kohl, N. E.; Gibbs, J. B.; Pan, B. S. Lung cancer cell lines harboring MET gene amplification are dependent on Met for growth and survival. *Cancer Res.* **2007**, *67*, 2081−2088.
(44) Baschnagel, A. M.; Kaushik, S.; Durmaz, A.; Goldstein, S.; Ong, I. M.; Abel, L.; Clark, P. A.; Gurel, Z.; Leal, T.; Buehler, D. Development and characterization of patient-derived xenografts from non-small cell lung cancer brain metastases. *Sci. Rep.* **2021**, *11*, No. 2520, DOI: 10.1038/s41598-021-81832-1.
(45) Ye, G.; Gallant, J.; Zheng, J.; Massey, C.; Shi, K.; Tai, W.; Odle, A.; Vickers, M.; Shang, J.; Wan, Y. The development of Nanosota-1 as anti-SARS-CoV-2 nanobody drug candidates. *eLife* **2021**, *10*, No. e64815, DOI: 10.7554/eLife.64815.
(46) SenthilKumar, G.; Fisher, M. M.; Skiba, J. H.; Miller, M. C.; Brennan, S. R.; Kaushik, S.; Bradley, S. T.; Longhurst, C. A.; Buehler, D.; Nickel, K. P.; et al. FGFR Inhibition Enhances Sensitivity to Radiation in Non−Small Cell Lung Cancer. *Molecular Cancer Therapeutics* **2020**, *19*, 1255−1265.
(47) Zeglis, B. M.; Lewis, J. S. The bioconjugation and radiosynthesis of 89Zr-DFO-labeled antibodies. *J. Vis Exp* **2015**, DOI: 10.3791/52521.
(48) Glumac, P. M.; Gallant, J. P.; Shapovalova, M.; Li, Y.; Murugan, P.; Gupta, S.; Coleman, I. M.; Nelson, P. S.; Dehm, S. M.; LeBeau, A. M. Exploitation of CD133 for the Targeted Imaging of Lethal Prostate Cancer. *Clin. Cancer Res.* **2020**, *26*, 1054−1064.

https://doi.org/10.1021/acs.bioconjchem.4c00019
Bioconjugate Chem. 2024, 35, 389−399